www.springer.com/41230
https://doi.org/10.1007/s41230-026-5263-6
Research & Development
Vol. 23 No. 3 May 2026
CHINA FOUNDRY

Microstructure and mechanical properties evolution of near-β alloy Ti-4Al-6Cr-5Mo-5Nb-*x*Ta

Jia-qi Hao[1], **Hong-ze Fang[1, 2], Xing-fang Xue[1], Ji-chang Yu[1], Bo-bo Li[2], Bao-hui Zhu[3, 4], and *Rui-run Chen[1, 2]

1. National Key Laboratory for Precision Hot Processing of Metals, Harbin Institute of Technology, Harbin 150001, China

2. Zhengzhou Research Institute, Harbin Institute of Technology, Zhengzhou 450000, China

3. Luoyang Ship Material Research Institute, Luoyang Shuangrui Precision Casting Titanium Industry Co., Ltd., Zhengzhou 471000, China

4. Ningxia Horizontal Titanium Industry Co., Ltd., Shizuishan 753000, Ningxia, China

Abstract: To meet the aerospace industry's demand for aircraft featuring high thrust-to-weight ratios and lightweight structures capable of operating in complex service environments, β titanium alloys with high specific strength and good plasticity have become a current research hotspot in the development of domestic fasteners. Based on the calculated Mo equivalent, the alloy composition Ti-4Al-6Cr-5Mo-5Nb is classified as a near-β titanium alloy within the titanium alloy design space. The microstructure is further controlled by adding alloy element Ta with a mass fraction of 0.4wt.%–2.0wt.%. Research results indicate that Ta dissolves completely in the matrix without forming new phases within the investigated range. As the Ta content increases, the proportion of the β phase increases significantly, the β grain diameter decreases markedly from 2.4 mm to 0.4 mm, and the α phase gradually coarsens. When adding 1.6wt.% Ta, the tensile strength and fracture toughness of the alloy reach the peak values of 735 MPa and 55 MPa·m$^{1/2}$, respectively.

Keywords: titanium alloy; Ta; microstructure; tensile strength; fracture toughness

CLC numbers: TG146.23 **Document code:** A **Article ID:** 1672-6421(2026)03-315-12

1 Introduction

High-performance near-β titanium alloys are critical structural materials in advanced aerospace and marine applications, driven by their exceptional strength-to-weight ratio[1-3]. The development of next-generation components requires an exceptional synergy of mechanical properties, particularly high levels of both strength and fracture toughness[4]. A fundamental challenge impeding this goal is the inherent strength-toughness trade-off, where conventional strengthening pathways often detrimentally affect fracture resistance[5-7]. Therefore, innovative alloy design strategies are essential to overcome this antagonistic relationship[8, 9].

Alloying with β-stabilizing elements is a proven approach to tailor the microstructure and mechanical properties of titanium alloys[10, 11]. Among these, tantalum (Ta) is a particularly compelling candidate[12]. As an isomorphous β-stabilizer, Ta effectively enhances the matrix strength via solid-solution strengthening[13, 14]. Crucially, its atomic radius is proximate to that of Ti, which minimizes lattice distortion and is thus beneficial for retaining toughness and ductility during strengthening[15-18]. This assertion is supported by first-principles calculations, which indicate a strong interatomic bonding between Ta and Ti[19], suggesting a significant potential for improving mechanical performance[20].

Our preliminary investigations identified the

***Rui-run Chen**

Professor, Doctoral Supervisor. He is a selected member of the "Youth Talent Support Program" of the China Association for Science and Technology. His research primarily focuses on electromagnetic cold crucible directional solidification technology; microstructure and property control of TiAl alloys and their composites; ultrasonic-assisted preparation of TiAl alloys for microstructure and property optimization; development of high-temperature, ultra-high-strength, and toughness titanium-based alloys; and the regulation of microstructure and properties of Ti and TiAl based alloys manufactured by additive manufacturing. To date, he has published more than 100 academic papers and has applied for or been granted over 50 national invention patents.

E-mail: ruirunchen@hit.edu.cn

****Hong-ze Fang**

E-mail: fanghongze@hit.edu.cn

Received: 2025-10-28; Revised: 2025-12-17; Accepted: 2026-02-08

Ti-4Al-6Cr-5Mo-5Nb alloy as a promising castable system, however, it exhibits a suboptimal strength-toughness balance that fails to meet the stringent performance targets. To address this limitation, the present study systematically investigates the influence of micro-alloying with Ta on this base alloy. The primary objective is to achieve a concurrent enhancement in strength and toughness by strategically tailoring the microstructure, specifically through the refinement and morphological control of the α-phase precipitates. This work elucidates the governing mechanisms by examining the evolution of phase constitution, microstructural features, and the resultant mechanical properties in the newly developed Ti-4Al-6Cr-5Mo-5Nb-*x*Ta alloys.

2 Materials and methodology

Alloys with nominal compositions of Ti-4Al-6Cr-5Mo-5Nb-*x*Ta (*x*=0, 0.4, 0.8, 1.2, 1.6, and 2.0, in wt.%) were prepared from high-purity starting materials. These included sponge Ti (≥99wt.%), Mo, Al, Cr, Ta (≥99wt.%), and a Ti-50Nb master alloy. The fabrication was conducted in a high-vacuum arc furnace, where each ingot was flipped and remelted four times to achieve a homogeneous distribution of the constituent elements.

The chemical compositions of the alloys were verified using an Axios-PW4400 X-ray spectrometer. Phase identification was performed using X-ray diffraction (XRD) with a Cu Kα radiation source. The phase transformation temperatures were determined via differential scanning calorimetry (DSC). The sample mass was approximately 200 mg, and it was heated to 1,000 °C at a heating rate of 10 °C·min^{-1}. For microstructural characterization, a suite of microscopy techniques was employed, including optical microscopy (OM, Olympus GX71), scanning electron microscopy (SEM, Merlin Compact), and transmission electron microscopy (TEM, FEI Talos F200X).

Mechanical properties were evaluated at ambient temperature using an Instron5569 universal testing machine. Uniaxial tensile tests were performed on dog-bone shaped specimens with a gauge section of 15 mm (length)×2.2 mm (width) ×2 mm (thickness). For fracture toughness evaluation, single-edge notched specimens with dimensions of 16 mm×4 mm×2 mm were utilized. Tensile and fracture toughness tests were performed at constant crosshead speeds of 1 mm·min^{-1} and 0.5 mm·min^{-1}, respectively. To ensure statistical reliability, all reported values are the average of at least three independent tests. The plane-strain fracture toughness (K_{IC}) value can be manifested as follows:

$$K_{IC}=\left(\frac{P_Q}{b}\right)\left(\frac{L}{W^{\frac{3}{2}}}\right)f\left(\frac{a}{W}\right) \quad (1)$$

$$f\left(\frac{a}{W}\right)=2.9\left(\frac{a}{W}\right)^{\frac{1}{2}}-4.6\left(\frac{a}{W}\right)^{\frac{3}{2}}+21.8\left(\frac{a}{W}\right)^{\frac{3}{2}}-37.6\left(\frac{a}{W}\right)^{\frac{7}{2}}+38.7\left(\frac{a}{W}\right)^{\frac{9}{2}} \quad (2)$$

where P_Q is the conditional load, S=16 mm is the loading span (with S=4W), W=4 mm is the width of the specimen. The sample thickness is denoted by b=2 mm, and a=2 mm represents the pre-crack length.

3 Results

3.1 Chemical composition of alloys with varing Ta content

The measured chemical compositions of the as-cast alloys are listed in Table 1. The results demonstrate that the actual elemental contents are in close agreement with the nominal compositions. This confirms that the vacuum arc melting process provided excellent control over the alloy chemistry, yielding ingots that are representative of the designed compositions and suitable for subsequent microstructural and mechanical analysis.

3.2 Phase constitution with varying Ta content

The phase constitution of the as-cast Ti-4Al-6Cr-5Mo-5Nb-*x*Ta alloys was characterized by X-ray diffraction (XRD), with the patterns presented in Fig. 1. The results indicate that all alloys are composed of a primary body-centered cubic (BCC) β phase and trace amounts of a hexagonal close-packed (HCP) α phase. The absence of any additional peaks confirms the complete solid solution of Ta within the alloy matrix.

Table 1: Chemical composition of selected alloys (wt.%)

Nominal composition	Measured composition					
	Ti	Al	Cr	Mo	Nb	Ta
0Ta	Bal.	3.92±0.12	6.04±0.06	4.91±0.17	5.09±0.09	-
0.4Ta	Bal.	4.05±0.12	5.86±0.06	4.88±0.17	4.89±0.09	0.42±0.01
0.8Ta	Bal.	3.88±0.12	5.93±0.06	4.95±0.17	5.07±0.09	0.85±0.01
1.2Ta	Bal.	3.81±0.12	5.98±0.06	4.99±0.17	4.82±0.09	1.17±0.01
1.6Ta	Bal.	4.07±0.12	6.01±0.06	5.07±0.17	4.99±0.09	1.64±0.01
2.0Ta	Bal.	4.01±0.12	5.92±0.06	5.01±0.17	4.92±0.09	2.02±0.01

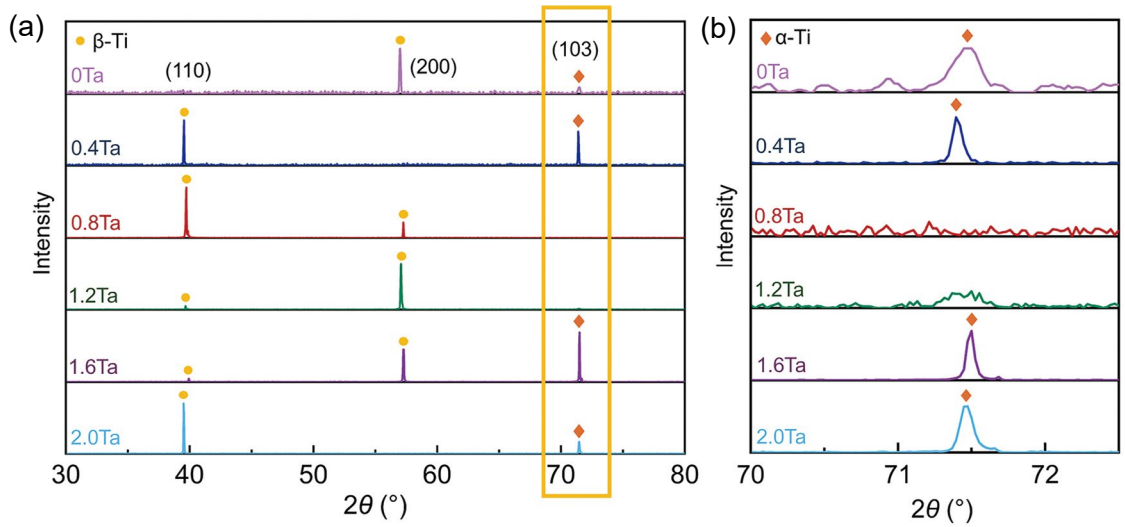

Fig. 1: XRD results of Ti-4Al-6Cr-5Mo-5Nb-*x*Ta alloys: (a) XRD pattern; (b) magnification of the yellow box area in Fig. 1(a)

A key observation from the X-ray diffractograms is a systematic shift of all peaks toward higher 2θ angles with increasing Ta content. As detailed in Fig. 1(a), the prominent β-(110) peak shifts from 39.46° to 39.93° as Ta concentration increases from 0 to 1.6wt.%. Similarly, the α-(103) peak shifts from 71.44° to 71.55° [Fig. 1(b)]. According to Bragg's Law [$2d\sin\theta=n\lambda$], this shift to higher diffraction angles corresponds to a decrease in the interplanar spacing (d-spacing), signifying a contraction of the unit cell lattice. This phenomenon can be attributed to the difference in atomic radii between the solute and solvent atoms. Ta acts as a substitutional element in the Ti matrix, forming a substitutional solid solution. Since the atomic radius of Ta (0.143 nm) is smaller than that of Ti (0.147 nm), the replacement of Ti atoms by smaller Ta atoms induces a lattice contraction. Consequently, this reduction in lattice parameters leads to the observed shift of diffraction peaks to higher 2θ angles. The low intensity of α-phase peaks in XRD reflects its low volume fraction (<10vol.%) in the β-dominated as-cast microstructure.

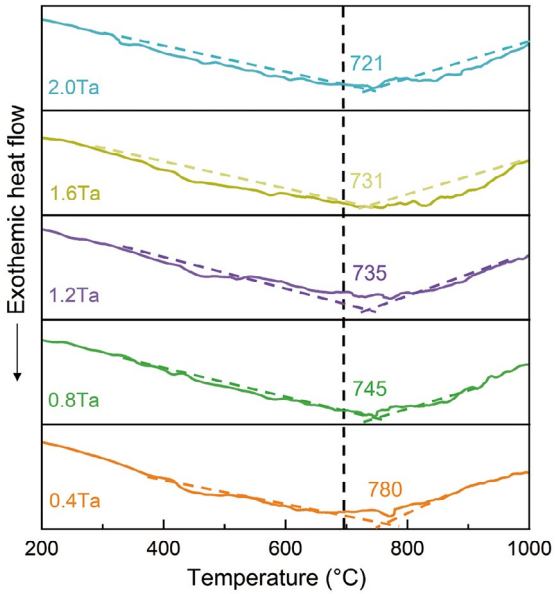

Fig. 2: DSC test results of Ti-4Al-6Cr-5Mo-5Nb-*x*Ta alloys

3.3 Phase transition temperature with varying Ta content

The phase transformation behavior of the Ti-4Al-6Cr-5Mo-5Nb-*x*Ta alloys was investigated using high-temperature differential scanning calorimetry (DSC), with the resulting thermograms presented in Fig. 2. During the heating cycle, each alloy exhibits a single, distinct exothermic peak, which corresponds to the α→β phase transformation. The β-transus temperature (T_β), taken as the peak temperature of this endotherm, shows a clear dependence on Ta content. The T_β is the highest for the 0.4Ta alloy, recorded at approximately 780 °C. As the Ta concentration is further increased to 2.0wt.%, the T_β systematically decreases to 721 °C, confirming the β-stabilizing effect of Ta. Conversely, during the cooling segment, no exothermic peaks corresponding to the β→α transformation, are observed in any of the alloys.

This absence can be attributed to several factors related to the experimental conditions and alloy characteristics. Firstly, the cooling rate employed in DSC (10 °C·min^{-1}) is relatively moderate, which may result in a sluggish and diffuse transformation that produces a broad, weak thermal signal difficult to detect above the baseline noise. Secondly, the strong β-stabilizing effect of the alloying elements (particularly Ta, Mo, Nb, and Cr) significantly suppresses the β→α transformation kinetics, potentially shifting the transformation to lower temperatures or requiring longer times to complete. Thirdly, in near-β titanium alloys with a high β-stabilizer content, the transformation may occur gradually over a wide temperature range rather than at a sharp transformation temperature, making it challenging to identify a distinct exothermic peak. Despite the absence of a clear peak during cooling, the presence of α phase in the as-cast microstructure (confirmed by XRD in Fig. 1 and SEM in Fig. 5) indicates that the β→α transformation does occur, but under the slow solidification and cooling conditions of arc melting rather than during the controlled DSC cooling cycle.

3.4 Microstructures and morphologies of β grains with varying Ta content

Figure 3 shows the macroscopic images of the as-cast Ti-4Al-6Cr-5Mo-5Nb-*x*Ta alloys, characterized by coarse β grains. Due to the limited magnification and resolution of camera-based imaging, the fine α-phase precipitates are not visible at this scale, and these images primarily reveal the overall β grain morphology and size. This structure dominated by large-sized β phases is a direct result of the strong β-stabilizing effect of alloying elements. The addition of Ta, an isomorphous β-stabilizer, plays a crucial role. Possessing a body-centered cubic (BCC) crystal structure identical to that of β-Ti, Ta exhibits complete solid solubility within the matrix. This characteristic not only decreases the β→α transformation temperature but also inherently prevents the formation of intermetallic compounds. Furthermore, the minimal tendency for segregation associated with Ta ensures a chemically homogeneous β-phase matrix upon solidification.

It is worth noting that the β grain morphology changes significantly with varying Ta content. As the Ta addition increases, the β grains gradually transform from slender columnar to equiaxed, accompanied by a continuous refinement in grain size. To quantitatively calculate the average grain size, the microstructure of the alloy was collected by multi-region and multi-view scanning pictures. The β grain size was determined using the equivalent circle diameter

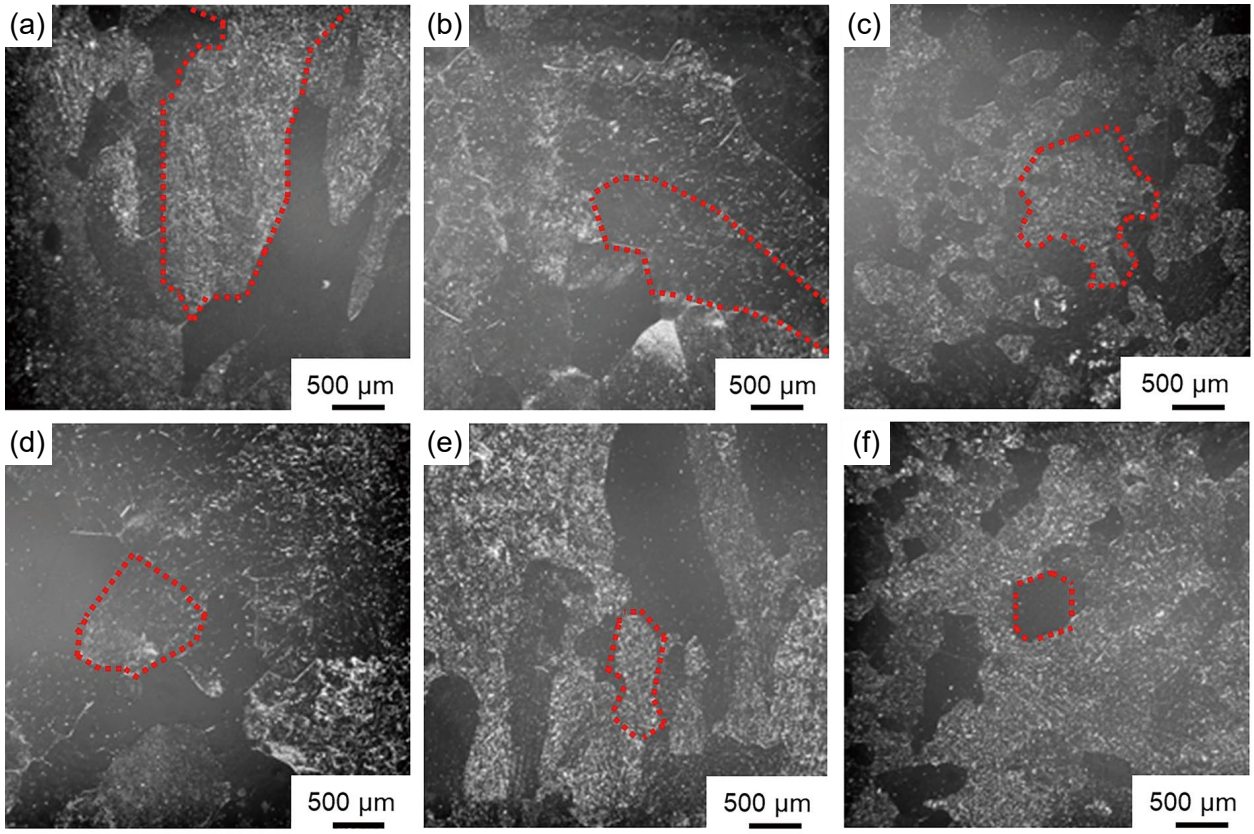

Fig. 3: Macroscopic images of β grains in Ti-4Al-6Cr-5Mo-5Nb-*x*Ta alloys obtained using a high-resolution camera: (a) 0Ta; (b) 0.4Ta; (c) 0.8Ta; (d) 1.2Ta; (e) 1.6Ta; (f) 2.0Ta

method. For each alloy composition, at least 50 grains were measured from different regions of the sample, and the average value was calculated as the representative grain size. The results are shown in Fig. 4. It is observed that as the content of Ta increases from 0 to 2.0wt.%, the β grain size decreases from 2.4 mm to 0.3 mm, representing a reduction of 87.5%.

To characterize the detailed microstructure and α-phase morphology within the β matrix at higher resolution, scanning electron microscopy (SEM) was employed. Figure 5 presents the high-magnification SEM images of the Ti-4Al-6Cr-5Mo-5Nb-*x*Ta alloys. It can be seen that only α and β phases are observed, confirming that Ta dissolves completely in the β-Ti matrix within the investigated composition range (0–2.0wt.% Ta) without forming any intermetallic compounds

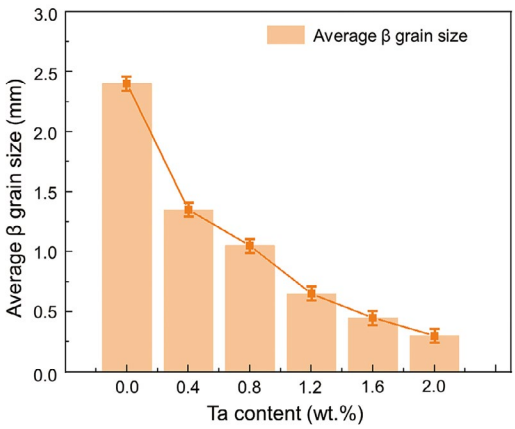

Fig. 4: Average β grain size

or other new phases. This behavior is consistent with Ta acting as an isomorphous β-stabilizer, as it shares the same BCC crystal structure as β-Ti. In addition, the cast structure of the alloy consists of coarse β grains and dispersed primary α phase (α_p) and secondary α phase (α_s). The primary α phase presents an elongated band, while the secondary α phase exhibits a finer, granular morphology. With the increase of Ta content, the β grains gradually transform from coarse columnar to fine equiaxed morphology, and the density of intragranularly distributed α phase increases. Microstructure observations also show that the size (both length and width) of the primary α phase (α_p) first increases and then decreases with increasing Ta content. Concurrently, the orientation of the α_p phase evolves from a disordered arrangement toward a more defined alignment, which improves the alloy's plasticity to a certain extent. The coarse primary α phase (α_p) can also hinder crack propagation, change the crack propagation path, increase the force required for crack propagation, and thus improve the fracture toughness of the alloy. Observations of the secondary α phase (α_s) show that its size remains relatively uniform. However, with increasing Ta content, the average size of the α_s phase exhibits a non-monotonic trend: initially increasing and then decreasing. It is worth noting that with the addition of Ta element, the α phases at grain boundaries become increasingly continuous and well-developed, reaching its maximum size at a Ta content of 1.6wt.%. At this composition, dislocation motion is more effectively impeded at the grain boundaries, which contributes to enhanced plasticity of the alloy.

3.5 Fracture toughness and tensile properties with varying Ta content

All alloys exhibit typical ductile behavior with distinct elastic and plastic deformation stages. Figure 6 shows the tensile fracture morphology of the designed alloys. As shown in Figs. 6(a) and (a'), the fracture surface of the alloy matrix without element Ta exhibits an obvious mixed fracture, displaying

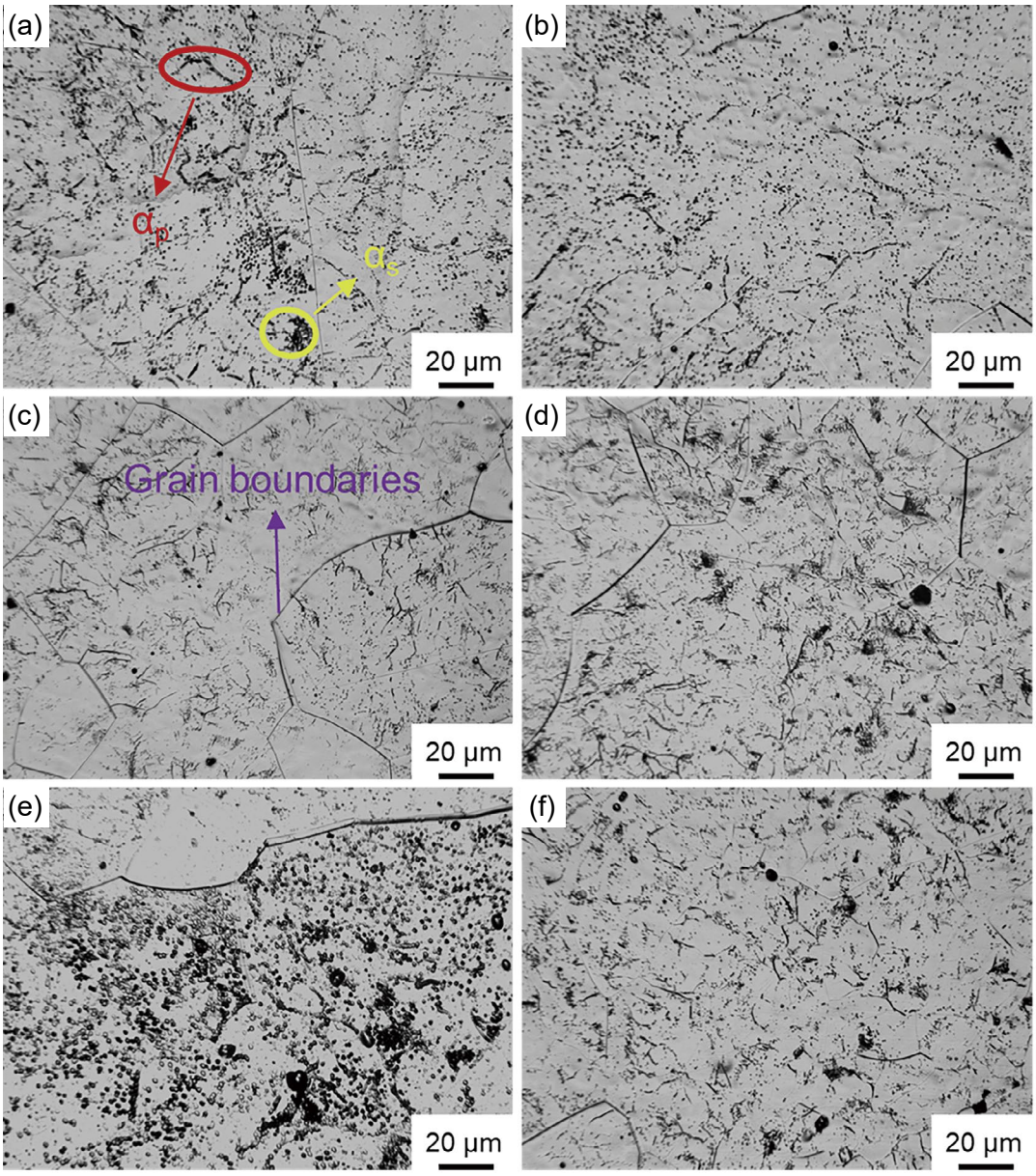

Fig. 5: SEM images of Ti-4Al-6Cr-5Mo-5Nb-*x*Ta alloys: (a) 0Ta; (b) 0.4Ta; (c) 0.8Ta; (d) 1.2Ta; (e) 1.6Ta; (f) 2.0Ta

characteristics of both brittle and ductile failure. With the addition of Ta element, the ductile fracture becomes dominate, and the fracture mechanism transitions to a typical microporous aggregation mode, indicating a significant improvement in the alloy's plasticity. In addition, dimples of different densities, phase interfaces, tearing edges, and some river patterns can be observed in the fracture surfaces of all alloys. With the increase of Ta element content, the size of the dimple gradually increases, reaching a maximum at 1.6wt.% Ta, indicating that the toughness reaches its peak at this composition. For the alloy without Ta addition, the fracture morphology exhibits an obvious tear edge. With the addition of Ta, this feature gradually diminishes and eventually disappears. However, when the Ta content reaches 2.0wt.%, the tear edge reappears, as shown in Fig. 6(f), indicating that excessive Ta adversely affects the alloy's plasticity, which is also confirmed by the tensile strength curve. At the same time, the interface of α/α and α/β phases are observed in Figs. 6(b) and (e). On one hand, these interfaces facilitate the propagation of cracks and improve the plasticity of the alloy; on the other hand, the refined α_s phase may hinder the propagation of microcracks and promote the improvement of alloy strength.

Figure 7(a) clearly illustrates the fracture behavior of the alloys with different Ta contents, and Fig. 7(b) shows their fracture toughness values. It is observed that the fracture toughness of the alloy first increases and then decreases with the increase of Ta. When the content of Ta is 0wt.%, the collective fracture toughness value of the alloy is 41 MPa·m$^{1/2}$, which is at a medium level in the near-β titanium alloy in as-cast state. When the Ta content increases to 1.6wt.%, the fracture toughness of the alloy reaches a peak of 55 MPa·m$^{1/2}$, which is 34.1% higher than that of 0Ta alloy. The increase of Ta content has a significant effect on the improvement of the fracture toughness of the alloy. However, when the Ta content reaches 2.0wt.%, the fracture toughness of the alloy decreases, due to the over-refinement of the α phase. An excessively fine α microstructure fails to effectively deflect the propagating crack, resulting in a relatively straight crack path. Consequently, less energy is dissipated during crack propagation, leading to a deterioration in fracture toughness. It is worth noting that with the increase of Ta element, both the strength and toughness of the alloy are significantly improved. Therefore, it is believed that addition of Ta has a positive effect on simultaneous enhancement of strength and toughness of near-β titanium alloys. Consequently, further research into heat treatment and thermal deformation of the designed Ti-4Al-6Cr-5Mo-5Nb-*x*Ta alloys holds significant promise for achieving optimal strengthening and toughening.

Tensile strength tests and fracture toughness tests were conducted. Figure 8 depicts the relationship between the

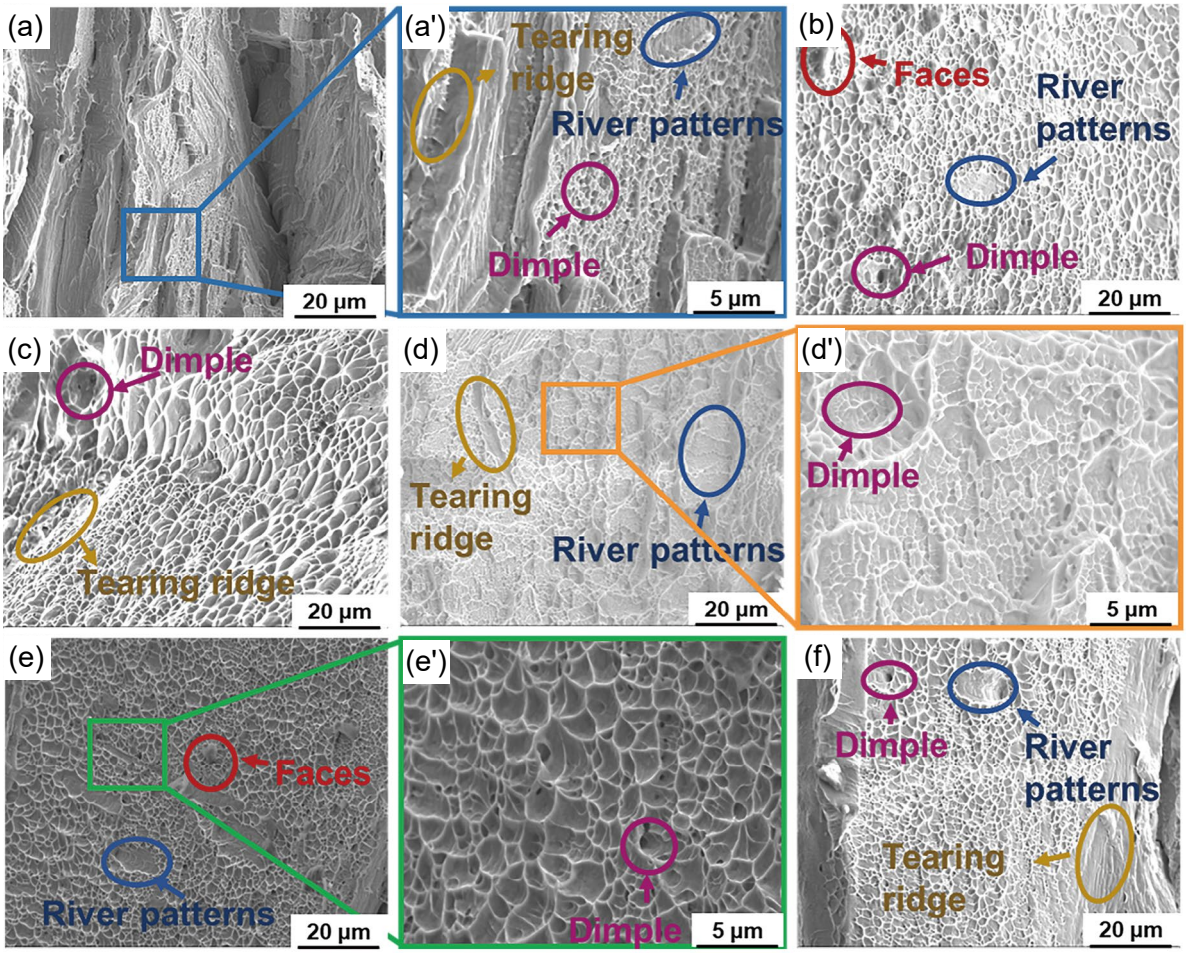

Fig. 6: Fracture morphology and crack propagation pathways of Ti-4Al-6Cr-5Mo-5Nb-*x*Ta: (a) and (a') 0Ta; (b) 0.4Ta; (c) 0.8Ta; (d) and (d') 1.2Ta; (e) and (e') 1.6Ta; (f) 2.0Ta

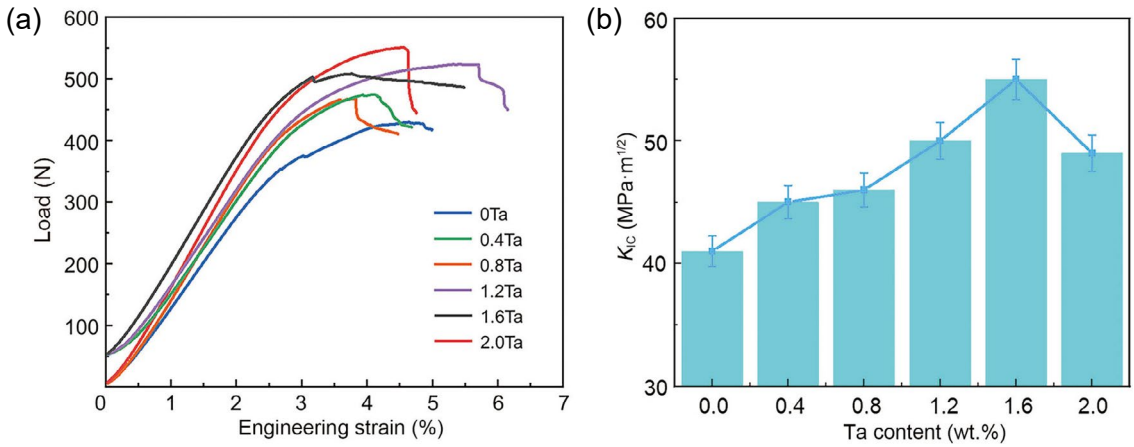

Fig. 7: Load-strain curves (a) and fracture toughness (b) of Ti-4Al-6Cr-5Mo-5Nb-*x*Ta

tensile properties of the designed alloy and Ta content, and the values of ultimate tensile strength (UTS), yield strength (YS), elongation (EL), and fracture toughness (K_{IC}) for the designed alloys are summarized in Table 2.

The influence mechanism of Ta content on the tensile strength of alloy is mainly due to microstructural modifications induced by varying Ta levels. With the increase of Ta content, the tensile strength of the alloy first increases and then decreases, which is similar to the change trend of elongation. The maximum tensile strength and elongation values of 0Ta alloy matrix are 694 MPa and 36.3%, respectively. When the Ta content increases to 1.6wt.%, both the tensile strength and elongation reach their peak values of 735 MPa and 50.1%, respectively, representing improvements of 5.9% and 38.0% compared to the 0Ta alloy.

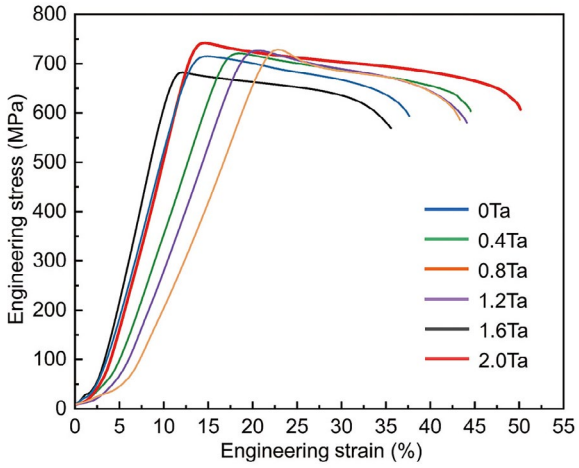

Fig. 8: Tensile properties of Ti-4Al-6Cr-5Mo-5Nb-*x*Ta alloys

Table 2: Tensile properties and fracture toughness of Ti-4Al-6Cr-5Mo-5Nb-*x*Ta alloys

Alloy	UTS (MPa)	YS (MPa)	EL (%)	K_{IC} (MPa·m$^{1/2}$)
0Ta	694±25	654±32	36.3±1.3	41±3
0.4Ta	707±28	668±42	38.1±1.4	45±4
0.8Ta	723±32	678±37	39.2±1.2	46±4
1.2Ta	725±21	682±29	40.1±1.3	50±2
1.6Ta	735±35	701±38	50.1±1.2	55±3
2.0Ta	729±26	699±24	44.6±1.4	49±3

The high elongation values achieved in these alloys reflect the combined effect of multiple deformation mechanisms active throughout the tensile deformation process. The substantial β grain refinement from 2.4 mm to 0.3 mm with Ta addition promotes more uniform strain distribution across the gauge length. Furthermore, the dispersed distribution of the α phase also plays a role in coordinating deformation and preventing premature failure.

3.6 Analysis of microstructure evolution during tensile deformation process

To further analyze the reasons for the high plasticity exhibited by the alloy during deformation, TEM images of the microstructure near the tensile fracture surface of the alloy with 1.6wt.% Ta addition were taken.

As shown in Fig. 9(a), the microstructure of the alloy consists of a β matrix, relatively coarse primary α phase (α_p), and dispersely distributed secondary α phase (α_s). High-magnification observation in Fig. 9(b) further reveals that the secondary α phase appears as fine needle-like or lamellar morphologies and distributed in a crisscross pattern within the β matrix. The calibration results of the corresponding selected area electron diffraction (SAED) patterns show that the α phase and the β matrix satisfy the classical Burgers orientation relationship: (110)β//(0001)α' and β//[11–20]α'. These dispersely distributed nanoscale α' phases, acting as hard particles, are the key to achieving precipitation strengthening and strength improvement of the alloy.

In the deformed structure, distinct deformation twins are observed in Fig. 9(c). The SAED pattern, acquired along the [123] zone axis of the BCC β phase, clearly shows both matrix diffraction spots and twin diffraction spots that exhibit mirror symmetry with respect to the (222) twin composition plane. This symmetric distribution of reflections is the direct crystallographic evidence for {112}<111> type deformation twins, which are commonly observed in BCC β-titanium alloys. The formation of twins is another important plastic deformation mechanism besides dislocation slip. It can

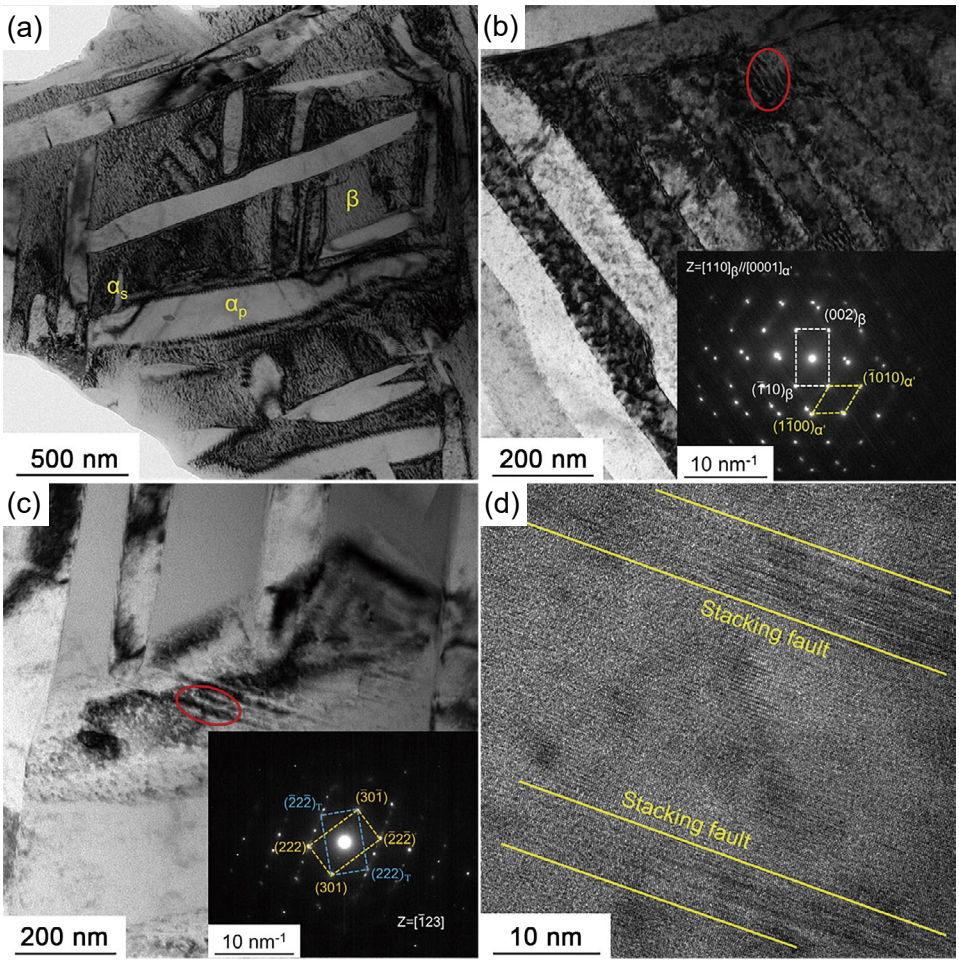

Fig. 9: Multi-scale TEM microstructures of deformed Ti-4Al-6Cr-5Mo-5Nb-1.6Ta alloy: (a) low-magnification bright-field TEM microstructure morphology; (b) secondary α' martensite and SAED patterns; (c) nano twinned structure and SAED pattern; (d) HRTEM image of stacking fault inside α' lamella

effectively coordinate plastic deformation and improve the ductility of materials. At the same time, as a new type of grain boundary, the twin boundary can impede the movement of subsequent dislocations, resulting in strong work hardening, which is crucial for achieving a simultaneous increase in both strength and plasticity.

Figure 9(d) reveals the presence of a high density of stacking faults in the matrix at the atomic scale. These stacking faults appear as local disruptions in the perfect periodic stacking structure of the crystal. In β-titanium alloys, the appearance of a large number of stacking faults usually indicates that the alloy has a low stacking fault energy (SFE)[21].

These TEM observations collectively point to the core role of Ta element in enhancing the properties of the alloy. As a β-stabilizing element, Ta dissolves into the β matrix, which significantly reduce the stacking fault energy of the system. On one hand, the low stacking fault energy promotes the initiation and propagation of deformation twins and activates the twinning-induced plasticity (TWIP) effect. This is the key reason why the alloy can simultaneously achieve high strength and high plasticity. On the other hand, the low stacking fault energy also makes dislocations tend to move in a planar slip mode, enhancing the interaction between dislocations and further improving the work hardening ability.

4 Discussion

4.1 Effect of Ta on phase content and size

As an isomorphous β-stabilizer with a BCC crystal structure identical to β-Ti, Ta theoretically has high solid solubility in the β phase[22]. Previous studies on Ti-Ta binary alloys have demonstrated extensive mutual solubility, particularly in the β phase field, so the addition of Ta greatly enhances the stability of β phase. In addition, as an element with a high melting point, large atomic radius, and slow diffusion rate, Ta hinders the transition process from β phase to α phase in the matrix. Therefore, with the increase of Ta content in the alloy, the phase transition process from the β phase to the α phase becomes difficult, therefore, the α phase content in the alloy decreases while the β phase increases. In addition, the solid-dissolved Ta atoms, acting as substitutional solutes in the matrix, promote the nucleation of the α phase while inhibiting its growth rate. The increase in Ta content can also promote the nucleation of α phase in more orientations, thereby reducing the size of α phase. From the measurement results of the phase transition temperature, it can be seen that as the Ta content increases, the phase transition temperature of the alloy decreases. Therefore, the generated α phase has sufficient time to grow, and when the Ta content exceeds 1.6wt.%, it will lead to a slight increase in the size of α phase.

4.2 Effect of Ta addition on β grain size

As a high melting point alloying element, Ta promotes the heterogeneous nucleation of β grains. This enhances competitive growth among the β grains, ultimately leading to their refinement. In addition, the increase in Ta content also causes the solidification front to produce component supercooling, and to a certain extent, it can also increase the nucleation points in the liquid phase region, resulting in the refinement of β grains. The microstructure refinement effect of Ta on titanium alloys is also related to its influence on the parameters related to the crystallization process of the alloy[21]. When the new phase crystallizes in a melt that satisfies the supercoolance condition, the uniform nucleation rate (N) can be calculated using Eq. (1):

$$N = K_{\mathrm{v}} \exp(-\Delta G_{\mathrm{k}} / kT) \exp(-\Delta G_{\mathrm{A}} / kT) \tag{1}$$

where K_{v} refers to a constant, ΔG_{k} stands for the nucleation energy, ΔG_{A} represents the activation energy of atoms transferred from liquid to nucleus, k is the Boltzmann constant, and T is the absolute temperature. The nucleation energy of new phase, ΔG_{k}, is described as follows:

$$\Delta G_{\mathrm{k}} = \frac{16\pi\sigma^3 T_{\mathrm{m}}}{3(L_{\mathrm{m}} \cdot \Delta T)^2} \tag{2}$$

where σ is the solid-liquid interfacial energy, T_{m} is the melting temperature, L_{m} is the latent heat of fusion per unit volume, and ΔT is the degree of supercooling. Ta, acting as a surface-active element, reduces the interfacial energy (σ), thereby lowering the nucleation barrier (ΔG_{k}) and significantly enhancing the nucleation rate (N).

4.3 Strength-toughness synergy mechanism of Ti-4Al-6Cr-5Mo-5Nb-*x*Ta alloys

The simultaneous enhancement of strength and toughness observed in the Ti-4Al-6Cr-5Mo-5Nb-*x*Ta alloys, particularly in the 1.6Ta composition, is a result of a sophisticated interplay of multiple strengthening and toughening mechanisms acting at different scales. The addition of Ta orchestrates a hierarchical microstructure optimized for mechanical performance, which can be elucidated through the combined effects of solid solution strengthening, grain boundary strengthening, precipitation strengthening, and deformation-induced twinning.

It can be seen from Figs. 3, 4, and 6 that the tensile strength and fracture toughness of the designed alloy exhibit a trend of first increasing, peaking at 1.6wt.% Ta, and then decreasing with further Ta addition beyond 1.6wt.%. This initial simultaneous improvement in strength and toughness is likely associated with the substitutional solid solution of Ta in the matrix, refinement of β grains, and the consequent increase in grain boundary area. The balanced microstructure, characterized by refined grains and uniformly distributed fine α-phase precipitates, contributes to a good synergy between strength and ductility. During plastic deformation, dislocations interact with grain boundaries, phase boundaries, and other dislocations, leading to work hardening that enhances strength. Simultaneously, the fine grain structure and dispersed α precipitates promote homogeneous strain distribution by providing multiple barriers that prevent severe strain localization. The BCC β phase offers multiple slip systems that facilitate dislocation motion redistribution through cross-slip mechanisms, which helps maintain ductility. This microstructural optimization enables the alloy to achieve both high strength through dislocation strengthening mechanisms and good ductility through distributed plastic deformation.

Ta element is a typical β stable element, it shows a crystal structure close to β-Ti when solid soluble in the matrix. Therefore, the addition of Ta to the near-β titanium alloy provides a pronounced solid solution strengthening effect. When an appropriate amount of Ta is added, it can form a stable solid solution with β-Ti, so that the crystal structure of Ti has a certain lattice distortion. This distortion creates internal stresses inside the alloy that impede the slippage and climbing of dislocations. This promotes an increase in the tensile strength of the alloy, an effect that can be estimated using the dislocation-solute elastic interaction equation[23]:

$$\sigma_{\mathrm{ss}} = \left(\Sigma_i B_i^{\frac{3}{2}} X_i \right)^{2/3} \tag{3}$$

where σ_{SS} represents the strength increment contributed by solid solution strengthening, B_i denotes the solid solution strengthening coefficient of the i-th alloying element, and X_i is the atomic concentration of the i-th alloying element.

In addition, the size of β grains varies with the increase of Ta content. The smaller the grain size, the greater the number of grain boundaries. As one of the strengthening methods, the role of grain boundary strengthening cannot be ignored. The more the grain boundaries, the greater the impediment to dislocations and the better the reinforcement. Grain boundary strengthening, σ_{GB}, is usually calculated using the classical Hall-Petch equation, which is proposed on the basis of the dislocation blocking model[24] in the form shown in Eq. (4):

$$\sigma_{\mathrm{GB}} = \frac{k}{\sqrt{d}} \tag{4}$$

where k is the Hall-Petch constant[25], which is 735 MPa·μm$^{1/2}$ for the Ti alloy substrate, and d represents the average β grain size.

It should be emphasized that although dislocation obstruction contributes to strength enhancement, excessive obstruction can indeed lead to crack initiation and embrittlement. The key to achieving good ductility lies in maintaining a balance where dislocations are moderately hindered to provide strengthening, but the microstructure still allows sufficient dislocation mobility and strain accommodation. In the experimental alloys, the fine grain size (reduced from 2,400 μm to 300 μm with 1.6wt.% Ta addition) and the dispersed fine α precipitates create a microstructure that achieves this balance. The grain boundaries and α/β interfaces not only strengthen the alloy by blocking dislocation transmission, but also facilitate strain accommodation through dislocation absorption and localized rearrangement, thus preventing the initiation and propagation of catastrophic crack formation. This is evidenced by the simultaneous increase in both ultimate tensile strength (from

694 MPa to 735 MPa) and elongation (from 36.3% to 50.1%) with Ta addition from 0 to 2.0wt.%.

TEM analysis in Fig. 9 reveals a high density of finely dispersed, acicular α-phase precipitates within the β matrix. These nano-scale precipitates act as potential pinning points for dislocation, leading to significant precipitation strengthening (σ_p). The resistance offered by these precipitates forces dislocations to bow out and bypass them via the Orowan mechanism. This process requires a higher applied stress to sustain plastic deformation and thus increasing the alloy's strength. The optimized size and distribution of the α phase at 1.6wt.% Ta likely provides the most effective precipitation strengthening effect without compromising ductility.

Most importantly, the key to the excellent strength-toughness synergy lies in the alloy's work-hardening behavior, which is directly linked to deformation mechanisms observed via TEM. In the deformed microstructure of the 1.6Ta alloy, a high density of deformation twins and stacking faults are observed. The presence of stacking faults indicates that the addition of Ta lowers the stacking fault energy (SFE) of the β matrix. A lower SFE facilitates the activation of twinning as a competitive deformation mechanism alongside dislocation slip. This twinning-induced plasticity (TWIP) effect plays a dual role: (a) It provides an additional deformation mode beyond conventional dislocation slip, significantly enhancing the strain accommodation capacity; (b) The newly formed twin boundaries act as dynamic barriers to subsequent dislocation motion, effectively refining the microstructure during deformation. This sustained high work-hardening rate is particularly important during the uniform elongation stage, as it delays the onset of necking and allows for substantial plastic deformation. Ultimately, the combination of grain refinement, solid solution strengthening, and the TWIP mechanism enables the alloy to achieve exceptional elongation values while maintaining a high ultimate tensile strength.

The improved plasticity observed in the Ta-containing alloys should not be attributed to severe dislocation obstruction, but rather to the microstructural refinement and the enhanced capacity for homogeneous plastic deformation. The fracture surface analysis (Fig. 7) shows typical ductile fracture characteristics with dimple structures, confirming that the alloys maintain good ductility through void nucleation, growth, and coalescence mechanisms rather than brittle fracture. This ductile fracture behavior is facilitated by the fine microstructure that promotes uniform strain distribution and delays the onset of necking. Therefore, the peak mechanical properties at 1.6wt.% Ta are not achieved by a single mechanism, but by a synergistic combination, as shown in Fig. 10. Refined β grains and solid solution strengthening provide a high baseline strength. As the material deforms, fine α precipitates offer strong resistance to dislocation motion (precipitation strengthening), while the activation of deformation twinning (TWIP effect) ensures high ductility and a remarkable capacity for work hardening. It is this multi-faceted, hierarchical strengthening and toughening strategy, orchestrated by the addition of Ta, that allows the alloy to overcome the conventional strength-toughness trade-off. When Ta content exceeds 1.6wt.%, the potential coarsening of the α phase and other subtle changes may disrupt this delicate balance, leading to a decrease in both strength and toughness.

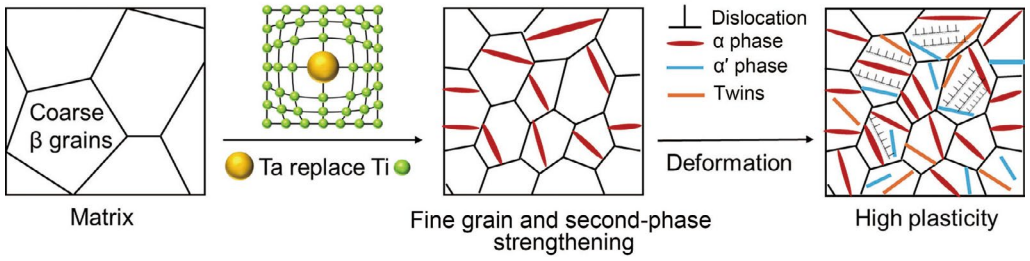

Fig. 10: Synergistic mechanism during deformation of Ti-4Al-6Cr-5Mo-5Nb-1.6Ta

Figure 11 presents a comparison of the strength and plasticity of common titanium alloys. Among these alloys, near-β titanium alloys represent the most optimal composition for attaining an ideal balance between strength and plasticity. They not only exhibit excellent strength but also possess high plasticity, rendering them highly suitable as raw materials for plastic processing. By employing appropriate processing techniques, near-β titanium alloys can achieve remarkable strength and toughness. The Ti-4Al-6Cr-5Mo-5Nb-1.6Ta alloy designed in this study demonstrates good strength, along with plasticity that far surpasses that of other common titanium alloy compositions. As such, it holds significant research value for realizing strength and toughness enhancement through plastic processing.

5 Conclusions

This study mainly analyzes and characterizes the as-cast microstructure, phase constitution, tensile strength, and fracture toughness of the designed Ti-4Al-6Cr-5Mo-5Nb-*x*Ta alloys. It systematically investigates the effect of Ta addition on properties of the alloys, and provides a basis for screening optimal compositions for subsequent thermal flux. The main conclusions are as follows:

(1) As the content of Ta increases from 0 to 2.0wt.%, no new phases form in the microstructure; Ta atoms are almost completely dissolved in the β phase, leading to an increase in β-phase fraction, while the α-phase size initially increases and then decreases.

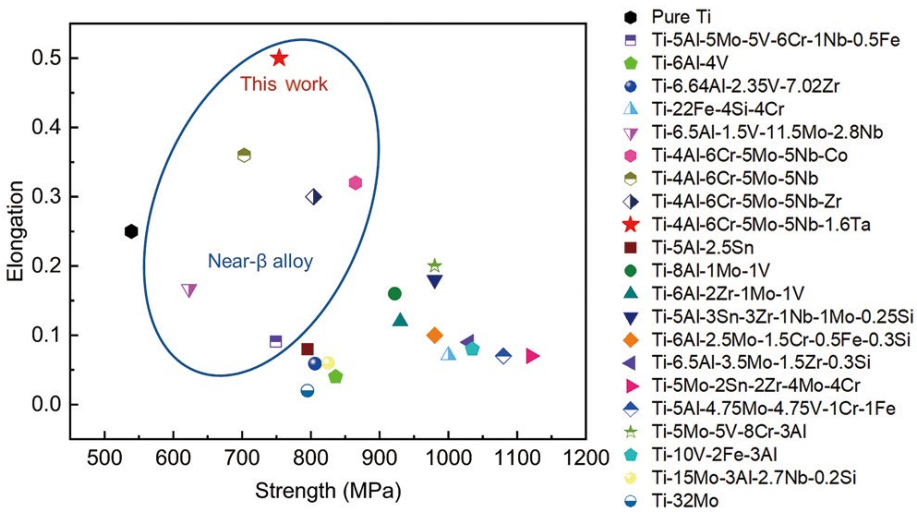

Fig. 11: Strength and plasticity properties of common titanium alloys[27-36]

(2) When the Ta content increases from 0 to 2.0wt.%, the β grain size decreases from 2.4 mm to 0.4 mm. Ta's large atomic radius hinders the growth of β grains, thereby limiting the transition from β phase to α phase.

(3) When the content of Ta increases from 0 to 1.6wt.%, the tensile strength and fracture toughness increase simultaneously, from 694 MPa and 41 MPa·$m^{1/2}$ to 735 MPa and 55MPa·$m^{1/2}$, respectively. When the Ta content exceeds 1.6wt.%, both the strength and toughness decrease.

(4) The superior strength-toughness combination achieved at 1.6wt.% Ta is attributed to the synergistic effects of solid solution strengthening, grain refinement strengthening, and precipitation hardening.

(5) The exceptional ductility is attributed to the TWIP effect, where Ta addition promotes deformation twinning through lowering stacking fault energy, enabling high work-hardening rate and overcoming the strength-ductility trade-off.

(6) The Ti-4Al-6Cr-5Mo-5Nb-1.6Ta alloy, with its optimal balance of high strength and excellent fracture toughness in the as-cast state, is identified as a highly promising candidate for subsequent thermomechanical processing to achieve even greater performance for demanding aerospace applications.

Acknowledgments

The authors are grateful to the financial support by the Major Science and Technology Achievement Transformation Project in Heilongjiang Province (ZC2023SH0075), the National Natural Science Foundation of China (52425401, U2441255, 52474377, and 52371015), the Young Elite Scientists Sponsorship Program by CAST (2021QNRC001), and the Henan Provincial Key Research and Development & Promotion Special Program (251111231400).

Conflict of interest

Prof. Rui-run Chen is an EBM of *CHINA FOUNDRY*. He was not involved in the peer-review or handling of the manuscript. The authors have no other competing interests to disclose.

References

[1] Pan J Y, Shi R H, Zhang Z H, et al. Composition-deformation mechanism-property machine learning model for strength-ductility improvement of β-type titanium alloys. International Journal of Plasticity, 2025, 194: 104461.

[2] Sass J O, Wenschuh J, Kosche J, et al. Computational evaluation of the impact of low-modulus beta-titanium alloys on stress shielding of tibial trays in cementless total knee replacements. Results in Engineering, 2025, 28: 107659.

[3] Boyer R R. An overview on the use of titanium in the aerospace industry. Materials Science and Engineering: A, 1996, 213: 103–114.

[4] Liang Z, Miao J, Brown T, et al. A low-cost and high-strength Ti-Al-Fe-based cast titanium alloy for structural applications. Scripta Materialia, 2018, 157: 124–128.

[5] Yang Z Y, Liu Z, Deng T S, et al. Effect of deep cryogenic treatment on microstructure and mechanical properties of near β titanium alloy after multi-directional loading. Journal of Alloys and Compounds, 2025, 1039: 183230.

[6] Cao Z H, Sun W, Ma Y J, et al. Strong and plastic metallic composites with nanolayered architectures. Acta Materialia, 2020, 195: 240–251.

[7] Yuan C, Liu D, Xu X C, et al. Altering tensile and crack initiation behavior in a metastable β titanium alloy via designing grain size and precipitates. Journal of Materials Research and Technology, 2024, 33: 39–50.

[8] Liu T Y, Lou Y C, Zhang S, et al. A novel Ti-5.55Al-6.70Zr-1.50V-0.70Mo-3.41Nb-0.21Si alloy designed using cluster-plus-glue-atom model for laser additive manufacturing. China Foundry, 2023, 20(4): 414–422.

[9] Zhang Y B, Xin S W, Zhang G J, et al. Investigation of tensile deformation behavior of a TWIP/TRIP metastable β titanium alloy at typical temperature. Part I: Room temperature. Materials & Design, 2024, 248: 113508.

[10] Postnikova M N, Kotov A D, Mosleh A O, et al. The influence of rapid-diffusive β-stabilizers on the microstructure formation and superplasticity of titanium-based alloys. Journal of Alloys and Compounds, 2024, 1002: 175065.

[11] Levine B R, Sporer S, Poggie R A, et al. Experimental and clinical performance of porous tantalum in orthopedic surgery. Biomaterials, 2006, 27: 4671–4681.

[12] Eisenbarth E, Velten D, Müller M, et al. Biocompatibility of β-stabilizing elements of titanium alloys. Biomaterials, 2004, 25: 5705–5713.

[13] Sina H, Iyengar S, Lidin S, et al. Reaction behavior and evolution of phases during the sintering of Ta-Al powder mixtures. Journal of Alloys and Compounds, 2016, 654: 103–111.
[14] Zhang Z Y, Cheng J J, Xie J Q, et al. Microstructural characterization and mechanical properties of (TiC+TiB)/TA15 composites prepared by an in-situ synthesis method. China Foundry, 2024, 21(2): 168–174.
[15] Hu S, Tan Y B, Shi W, et al. Microstructure, texture evolution and mechanical behavior of Ti-3.5Al-5Mo-4V titanium alloy during hot rolling in a β field. Materials Today Communications, 2022, 31: 103506.
[16] Zhu Z H, Liu T H, Chen Z P, et al. High-strength Ti-Al-V-Zr cast alloys designed using α and β cluster formulas. China Foundry, 2023, 20(1): 23–28.
[17] Zhang T, Wei D, Lu E, et al. Microstructure evolution and deformation mechanism of α+β dual-phase Ti-*x*Nb-yTa-2Zr alloys with high performance. Journal of Materials Science & Technology, 2022, 131: 68–81.
[18] Mao C, Yu W, Jin M, et al. Mechanobiologically optimized Ti-35Nb-2Ta-3Zr improves load transduction and enhances bone remodeling in tilted dental implant therapy. Bioactive Materials, 2022, 16: 15–26.
[19] He B, Shao W P, Tian X J, et al. Surface grain formation mechanism in the laser remelting molten pool of a near-β titanium alloy. Materialia, 2022, 24: 101521.
[20] Song Y, Xu D S, Yang R, et al. Theoretical study of the effects of alloying elements on the strength and modulus of β-type bio-titanium alloys. Materials Science and Engineering: A, 1999, 260: 269–274.
[21] Wen D, Titus M S. First-principles study of Suzuki segregation at stacking faults in disordered face-centered cubic Co-Ni alloys. Acta Materialia, 2021, 221: 117358.
[22] Genin K, Epifano E, Gheno T, et al. Effects of Al and refractory alloying elements (W, Ta and Hf) on oxidation kinetics, oxygen dissolution and diffusion in titanium alloys. Corrosion Science, 2024, 237: 112330.
[23] Weiss I, Semiatin S L. Thermomechanical processing of beta titanium alloys – An overview. Materials Science and Engineering: A, 1998, 243: 46–65.
[24] Souza P M, Sivaswamy G. Constitutive modelling and processing map of Ti-10V-2Fe-3Al β titanium alloy. International Journal of Mechanical Sciences, 2022, 216: 106975.
[25] Vasudevan V K, Court S A, Kurath P, et al. An analysis of the forgeability of Ti-10V-2Fe-3Al β titanium alloy using a combined Estrin Mecking and Avrami material constitutive model. Scripta Metallurgica, 1989, 23: 467–469.
[26] Chong Y, Deng G Y, Gao S, et al. Yielding nature and Hall-Petch relationships in Ti-6Al-4V alloy with fully equiaxed and bimodal microstructures. Scripta Materialia, 2019, 172: 77–82.
[27] Wang W, Chen C, Zhao R, et al. A laser additive manufactured metastable Ti-10V-2Fe-3Al β-titanium alloy: Microstructure, mechanical properties, and deformation mechanisms. Materials Science and Engineering: A, 2024, 890: 145863.
[28] Wang Z, Zhang H, Wang S, et al. A machine learning method based on TPE-XGBoost model for TRIP/TWIP near-β titanium alloy design. Materials Today Communications, 2024, 41: 110309.
[29] Feng T, Pan Z, Li N, et al. Achieving an excellent combination of strength and ductility in metastable β titanium alloys via coupling isothermal ω phase and TRIP/TWIP effects. Materials Characterization, 2024, 218: 114531.
[30] Giroud T, Villechaise P, Naït-Ali A, et al. Anisotropy in tensile properties of a high strength metastable β titanium alloy. Materials & Design, 2024, 247: 113401.
[31] Li Z, Huo Z, Zhao X, et al. Effect of external magnetic field on microstructures and mechanical properties of Ti-2Al-1.5Mn titanium alloy resistance spot welds. Journal of Manufacturing Processes, 2024, 124: 1273–1284.
[32] Huang D, Lian Z, Zhao Z. Isothermal β grain growth kinetics and mechanical properties of Ti-351 titanium alloy. Materials Today Communications, 2024, 40: 109896.
[33] Guo M, Huang T, Luo T, et al. Manipulation of the α-phase precipitation behavior through dual-aging treatment and its correlation with mechanical properties in a metastable β titanium alloy. Journal of Alloys and Compounds, 2024, 1005: 175891.
[34] Zeng C, Zhao Y, Wang H, et al. Microstructural evolution and mechanical property of high-strength metastable β titanium alloy joint via electron beam welding. Journal of Materials Research and Technology, 2024, 33: 9166–9179.
[35] Zhang F, Feng J, Xiang W, et al. Microstructure evolution, grain refinement, and mechanical properties of a metastable β titanium alloy during cold rolling and recrystallization annealing. Materials Characterization, 2024, 208: 113632.
[36] Liu X, Ren X, An X, et al. The effects of forging strategies on microstructures and mechanical properties of a Ti-5Al-5Mo-5V-1Cr-1Fe near β-titanium alloy. Journal of Materials Research and Technology, 2024, 32: 3258–3268.